Tectonophysics 493 (2010) 222–235

Contents lists available at ScienceDirect

Tectonophysics

journal homepage: www.elsevier.com/locate/tecto

Dependency of supershear transition and ground motion on the autocorrelation of initial stress

Jan Schmedes [a,b,*], Ralph J. Archuleta [a,b], Daniel Lavallée [a]

[a] Institute for Crustal Studies, UC Santa Barbara, USA
[b] Department of Earth Science, UC Santa Barbara, USA

ARTICLE INFO

Article history:
Received 29 September 2009
Received in revised form 11 May 2010
Accepted 16 May 2010
Available online 23 May 2010

Keywords:
Dynamic rupture
Supershear propagation
Heterogeneous fault properties
Strong ground motion
Transition to supershear propagation
Isochrone analysis

ABSTRACT

Theoretical and observational studies show that earthquakes on strike–slip faults can have rupture speeds exceeding the shear wave speed. Due to the close relationship between the rupture velocity and the radiated wave field, it is important to understand the conditions leading to supershear ruptures and their effect on the resulting ground motion. We compute dynamic strike slip ruptures in a 3D elastic half space using heterogeneous frictional properties on faults that are 60 km long. We use a grid spacing of 60 m allowing us to compute ground motion for frequencies from 0 to 5 Hz. We analyze the resulting ground motion using isochrones to explain phenomena we observe. We model the amplitudes of the initial shear stress as a self-similar random field with Cauchy distributed amplitudes. The wavenumber amplitude spectrum of initial stress decays as a power law with exponent ν that controls the decay and the spatial correlation of the initial stress. The faster the decay (corresponding to larger value of ν), the more correlated is the stress on the fault, i.e., the stress field appears spatially smoother. The strength on the fault is computed under the assumption of a constant *S*-factor, where *S* is the ratio of strength excess over stress drop. On a fault with uniform strength and stress drop the *S*-factor has to be less than a critical value for the supershear transition to occur. For models with heterogeneous initial stress we find that both the *S*-factor and the value of the spectral decay constant ν affect the occurrence of supershear rupture. We observe that for a given, but small enough, *S*-factor a smooth model ($\nu \geq 2$) can run at supershear speed while a rough model ($\nu \sim 1$) will rupture at subshear speeds for the same *S*-factor. Based on the theory of fracture, a non-dimensional number κ was introduced to quantify the condition when a transition to supershear rupture velocity can occur during an earthquake. Transition will occur when κ exceeds a critical value. We introduce a modified dimensionless parameter κ_{ac} that is based on the original parameter κ. The parameter κ_{ac} incorporates a length scale W_{ac} that reflects the degree of the autocorrelation of the stress field. We compute κ_{ac} for a large number of available dynamic ruptures that propagate at subshear and supershear speeds and find: i) there is a critical value $\kappa_{ac}^{(c)}$ below which all ruptures propagate subshear; ii) for values larger than $\kappa_{ac}^{(c)}$ there is only a finite probability that the rupture goes supershear, i.e. it is a necessary but not a sufficient condition for the occurrence of supershear rupture propagation.

1. Introduction

Based on a source model computed for the 1979 Imperial Valley earthquake Archuleta (1984) first proposed supershear rupture propagation as a potential mechanism to explain observed strong motion data. Spudich and Cranswick (1984) also inferred a supershear rupture for a segment of the Imperial Fault based on the phase velocity of pulses recorded on a linear array of accelerometers in the Imperial Valley. Supershear propagation had been developed in analytical studies by Burridge (1973) and Freund (1979). It was observed in numerical studies by Andrews (1976) and Day (1982). Wu et al. (1972) and Johnson et al. (1973) reported on laboratory experiments from which they inferred supershear propagation. Rosakis et al. (1999) were the first to observe the Mach cone of a supershear rupture in laboratory experiments that definitively showed the existence of supershear propagation for frictional shear sliding. More recently, supershear rupture propagation has been inferred for additional earthquakes, for example, the 1999 Izmit earthquake (Bouchon et al., 2001), the 2001 Kunlun earthquake (Bouchon and Vallée, 2003; Robinson et al., 2006) and the 2002 Denali Fault earthquake (Dunham and Archuleta, 2004; Ellsworth et al., 2004). A review of supershear velocity in seismology can be found in a paper by Bouchon in this volume. Besides source models obtained through kinematic inversions, researchers also linked other observations to the occurrence of supershear rupture. Among them are missing aftershocks in segments that potentially ruptured at supershear speed (Bouchon and Karabulut, 2008), and cracks occurring off the fault

* Corresponding author. Now at Upstream Research Company, ExxonMobil, USA. Tel.: +1 805 636 4955.
E-mail address: jasch@crustal.ucsb.edu (J. Schmedes).

0040-1951/$ – see front matter © 2010 Elsevier B.V. All rights reserved.
doi:10.1016/j.tecto.2010.05.013

(Bhat et al., 2007). These cracks are attributed to the Mach cone that is produced when the rupture propagates faster than the shear wave speed. Supershear ruptures have the capability to transport large ground motion at distances much further off the fault than subshear ruptures (Andrews, this volume; Dunham and Archuleta, 2005; Dunham and Bhat, 2008).

In view of getting a better assessment of seismic hazard, it is crucial to better understand physical conditions that will facilitate supershear rupture. For instance, Bouchon (2008) suggests that supershear propagation favors fault segments with a simple geometry, i.e., straight segments of faults. On such fault segments in a uniform stress field, we might expect that the shear stress is highly correlated. In the stochastic model used to generate the initial stress that will be discussed below, a highly correlated shear stress implies a rather large value for the parameter ν controlling the amount of spatial correlation (the power spectrum of the initial stress is proportional to $k^{-\nu}$ with k being the radial wavenumber). This is based on the formulation that the stress drop is attenuated as a power law in the Fourier domain (Andrews, 1980). Empirical evidence supports this hypothesis (e.g., Lavallée et al., 2006).

In the first part of this paper, we study and quantify how the spatial correlation of the initial stress constrains the transition to supershear propagation in dynamic rupture simulations. Later, we investigate the ground motion resulting from different stress fields. For this purpose we compare ground motion for subshear and supershear ruptures and use isochrones (Bernard and Madariaga, 1984; Spudich and Frazer, 1984) to explain phenomena we observe.

Aagaard and Heaton (2004) used heterogeneous kinematic rupture models to study the influence of subshear and supershear rupture propagation on ground motion. Bizzari et al. (2010) study ground motion using heterogeneous dynamic rupture models that propagate at supershear speed. One important difference between their rupture models and the rupture models computed in this study is that their faults intersect the free surface while our faults are buried. Bizzari et al. (2010) focus on the ground motion, in particular the high frequency content, resulting from heterogeneous dynamic rupture models. They find an enriched high frequency content for supershear rupture models compared to subshear rupture models, consistent with the conclusions by Bizzari and Spudich (2008). While we also will compare ground motion resulting from subshear and supershear ruptures, we are also interested in the influence of the autocorrelation of stress on the transition from subshear to supershear rupture speed.

2. Characterizing the transition to supershear velocity

To date dynamic rupture studies investigating the transition to supershear propagation speed have used homogeneous (Madariaga and Olsen, 2000; Dunham, 2007) or simple heterogeneous (e.g., rectangular barriers, Day, 1982) initial stress models (Dunham et al., 2003; Liu and Lapusta, 2008). We extend such studies to self-similar random models that incorporate spatial fluctuations of stress over a continuum range of length scales as postulated in Andrews (1980). In these models, the power spectrum is asymptotically attenuated according to a power law with exponent ν (Lavallée and Archuleta, 2003; Lavallée, 2008). The power spectrum of the initial stress is illustrated in Fig. 1.

Besides the initial shear stress, the seismic S-factor (Eq. (1)) (Andrews, 1976; Das and Aki, 1977) is identified as an important parameter that affects the occurrence of supershear propagation for homogeneous models (Dunham, 2007).

$$S = \frac{\tau_p - \tau_0}{\tau_0 - \tau_d} \tag{1}$$

The parameter τ_p corresponds to the strength (peak stress), τ_0 to the initial stress, and τ_d to the dynamic sliding stress (Fig. 1). Dunham (2007) showed that for $S > 1.19$ there is no supershear if the initial stress is homogeneous on the fault in a half space. However, even for simple heterogeneous initial stress models (barriers) Liu and Lapusta (2008) demonstrated that transition to supershear is possible for larger values of S if the rupture encounters a favorable heterogeneity.

Based on fracture mechanics, Madariaga and Olsen (2000) used a dimensionless parameter κ (Eqs. (2a) and (2b)) to distinguish between the different regimes characterizing the propagation of rupture during an earthquake: no propagation, subshear or supershear propagation:

$$\kappa = \frac{(\tau_0 - \tau_d)^2 W}{\mu(\tau_p - \tau_d) d_c} \tag{2a}$$

with μ as the shear modulus, W as the half width of the fault and d_c as the critical slip weakening distance (Fig. 1). Note, that κ can be written as a function of the S-factor (Andrews, 1976; Day, 1982):

$$\kappa = \frac{\tau_0 - \tau_d}{\mu} \frac{1}{1+S} \frac{W}{d_c} \tag{2b}$$

Madariaga and Olsen (2000) show there is supershear propagation if κ exceeds a critical value $\kappa^{(c)}$. Dunham (2007) shows that this critical value depends on S. It should be noted that these formulations were developed for simple homogeneous initial conditions.

Of all parameters involved in the definition of κ, there is still a question about the choice of the proper "characteristic fault length" to represent W for a heterogeneous model. This will be discussed in detail in a section dedicated to an alternative definition of κ. The definition of this new parameter κ_{ac} also depends on the autocorrelation of the initial stress. To validate the new formulation of κ_{ac} and determine empirically the critical κ_{ac} value $\kappa_{ac}^{(c)}$ that separates subshear and supershear ruptures, we use about 300 dynamic subshear and supershear ruptures (Schmedes et al., 2010), plus six ruptures computed for a 300 km strike–slip fault embedded in a 3D velocity model of Southern California (Dalguer et al., 2008; Olsen et al., 2009). It should be noted that our database includes models computed for different classes of initial stress (thus differing from the stochastic stress model described above), different models of strength (for example variable S) and different heterogeneous slip weakening distances. Hence it is an appropriate data set in order to test our proposed definition of κ_{ac}.

3. Model setup

We use a parallel MPI (message passing interface) version of the finite element code of Ma and Liu (2006) to compute our dynamic ruptures. A slip weakening friction law (Ida, 1972) is used (Fig. 1), but alternative friction laws are also considered. We perform our computation for a simple half space (P-wave speed $V_p = 5.2$ km/s, S-wave speed $V_s = 3.0$ km/s and density $\rho = 3.0$ kg/m^3) in which a vertical rectangular 60 km long and 15 km wide fault is buried 600 m below the free surface. We do not consider surface ruptures here because we are mainly interested in the influence of the initial stress field. Rupturing the free surface will complicate the situation as it can lead to supershear rupture propagation (Kaneko et al., 2008; Kaneko and Lapusta, this volume). We use a grid spacing of 60 m, which enables us to analyze the ground motion up to 5.0 Hz.

Initial shear stress is spatially heterogeneous on the fault. We compute an initial stress using an approach in which the 2D power spectrum of initial shear stress is attenuated according to a power law with exponent ν (Lavallée and Archuleta, 2003; Lavallée, 2008). The power spectrum of the initial stress is proportional to $k^{-\nu}$, where k is the 2D radial wavelength number. We use exponents $\nu = 1$, 2, 3 and 4 (examples are illustrated in Fig. 2). The larger the exponent ν is, the

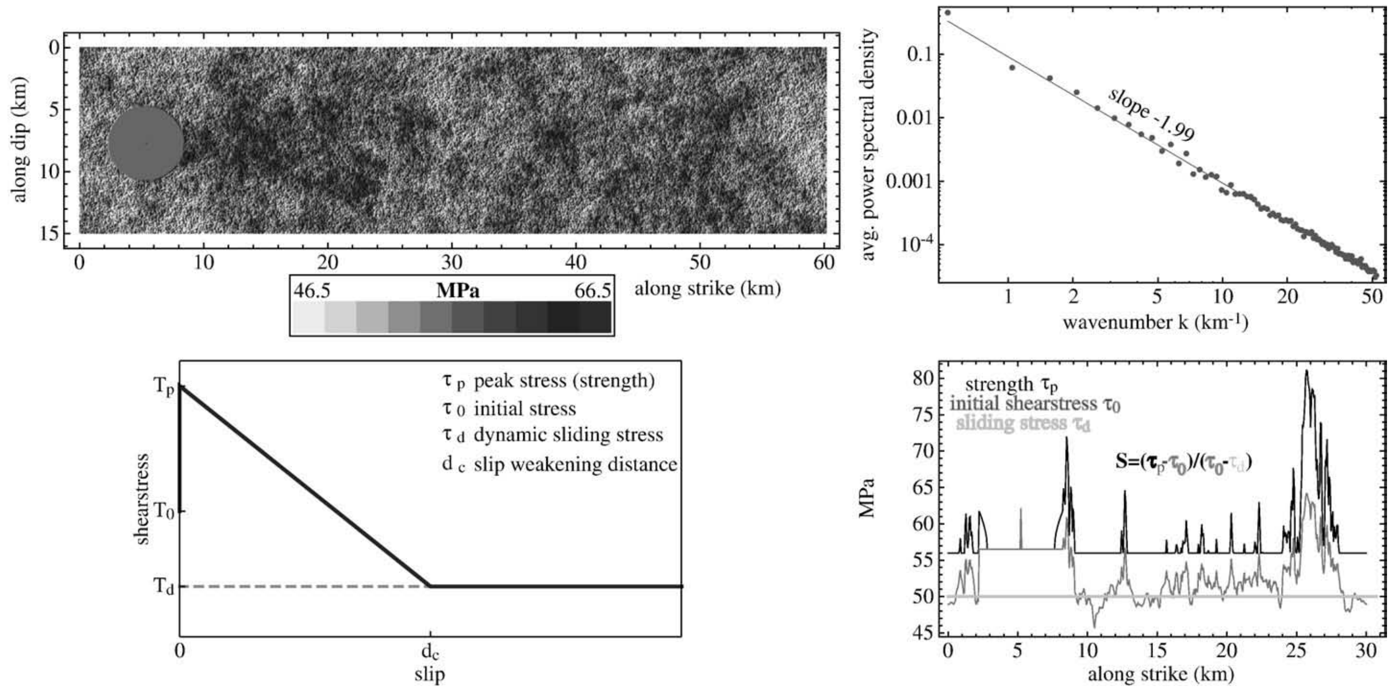

Fig. 1. Upper row: example of initial shear stress field with power spectral decay of 2 projected on the fault plane (left). The circle with constant initial shear stress is the nucleation region. The sliding friction is 50 MPa; average normalized power spectral density (right). The blue points are computed by averaging the power spectrum of the initial shear stress field along circles with constant κ. The line is fitted through the points. Lower row: Linear slip weakening friction law (left); Along strike profiles of sliding stress, initial shear stress and strength computed using constant *S*-factor (right). The profiles are through the middle of the fault, more precisely, through the point at which the perturbation in initial stress is applied that triggers the spontaneous rupture (blue peak in constant region at about 5 km along strike).

more the stress is correlated. Furthermore, for larger v the stress appears smoother because there is less energy at high wavenumbers.

In our stochastic model, the stress amplitude is distributed according to a Cauchy law (Lavallée and Archuleta, 2003; Lavallée et al., 2006; Liu et al., 2006; Schmedes et al., 2010). For all exponents v that describe the correlation, we ensure that the stress fields have identical amplitude distributions of initial stress. This guaranties that the initial stress models differ only in the amount of spatial autocorrelation characterized by the parameter ν. It is important to note that ν represents the power spectral decay not the Fourier spectral decay (which is $\nu/2$) often used in seismological literature. For instance, the heterogeneous rupture discussed in Bizzari et al. (2010) has a Fourier spectral decay of -1 for initial stress, i.e., $\nu = 2$ in our notation. The Fourier spectral decay in slip using our notation would be $\nu/2+1$.

The static coefficient of friction (shear strength if multiplied by the normal stress) is spatially heterogeneous on the fault. This is achieved by using a constant *S*-factor (Andrews, 1976; Das and Aki, 1977). We use $S = 0.6$, 0.8, 1.0, 1.2, and 1.4. We chose to use a constant *S*-factor because a) a comparison to homogeneous ruptures can be made; b) it enables us to analyze the transition to supershear velocity as a function of two independent parameters, ν and S. Thus one can isolate the dependence on ν when S is constant and vice versa. In the last section we also consider ruptures with variable S.

To ensure the ruptures are causal and no triggering occurs ahead of the rupture front, we prescribe a minimal value for the strength drop $\tau_p - \tau_d$. Because no region of the fault is expected to have zero strength before an earthquake, we use a finite positive value. This does yield a larger *S*-factor at the locations with small initial stress than the *S*-factor we initially used.

We nucleate the ruptures by setting the initial shear stress in a circular area (radius 2.7 km) equal to the strength. The center point is elevated above the level of strength (Fig. 1). This yields a slow nucleation that mimics a triggered rupture (Campillo et al., 2001). As pointed out by Liu and Lapusta (2008), this feature is important to prevent nucleation of a daughter crack in front of the main crack that results from a too forceful initial nucleation.

The rupture velocity is computed as the norm of the inverse numerical gradient of the rupture times. As a measure of supershear propagation, we compute the fraction of the total area of the fault where the rupture velocity exceeds the Eshelby speed $\sqrt{2}V_s$. We use the Eshelby speed because if we use only an area where we compute a velocity that exceeds the shear wave speed, the result may not be reliable due to numerical artifacts in computing the rupture velocity. These numerical artifacts generally lead to points on the fault that would be assigned supershear propagation speed even though the rupture is subshear. This happens because not only are the rupture times sampled discrete in space, but the rupture front also advances only in discrete time steps during the computation of the dynamic rupture. But the probability of a point getting assigned a propagation speed above the Eshelby speed due to numerical artifacts is low.

As discussed in Section 4.1, stable supershear propagation manifests itself in a second maximum around the Eshelby speed in the probability density of rupture velocity. Subshear ruptures have uni-modal rupture velocity distribution with the mode at sub-Rayleigh speed. Supershear ruptures have a bi-modal distribution with one sub-Rayleigh and one supershear mode. In the extreme case of a pure supershear rupture the distribution would be uni-modal, but the mode would be above the Eshelby speed.

4. Rupture propagation

4.1. Fixed S-factor, variable v

First we compare the rupture dynamics for the four initial stress models based on exponents $\nu = 1, 2, 3,$ and 4 (Fig. 2) and all with an *S*-factor of 1.4. All four models were computed from the same white noise field. Note, that in the way the models are constructed, i.e., same marginal distributions of stress and strength, same d_c, and same geometry, all models have the same value of κ. Fig. 3 shows final slip,

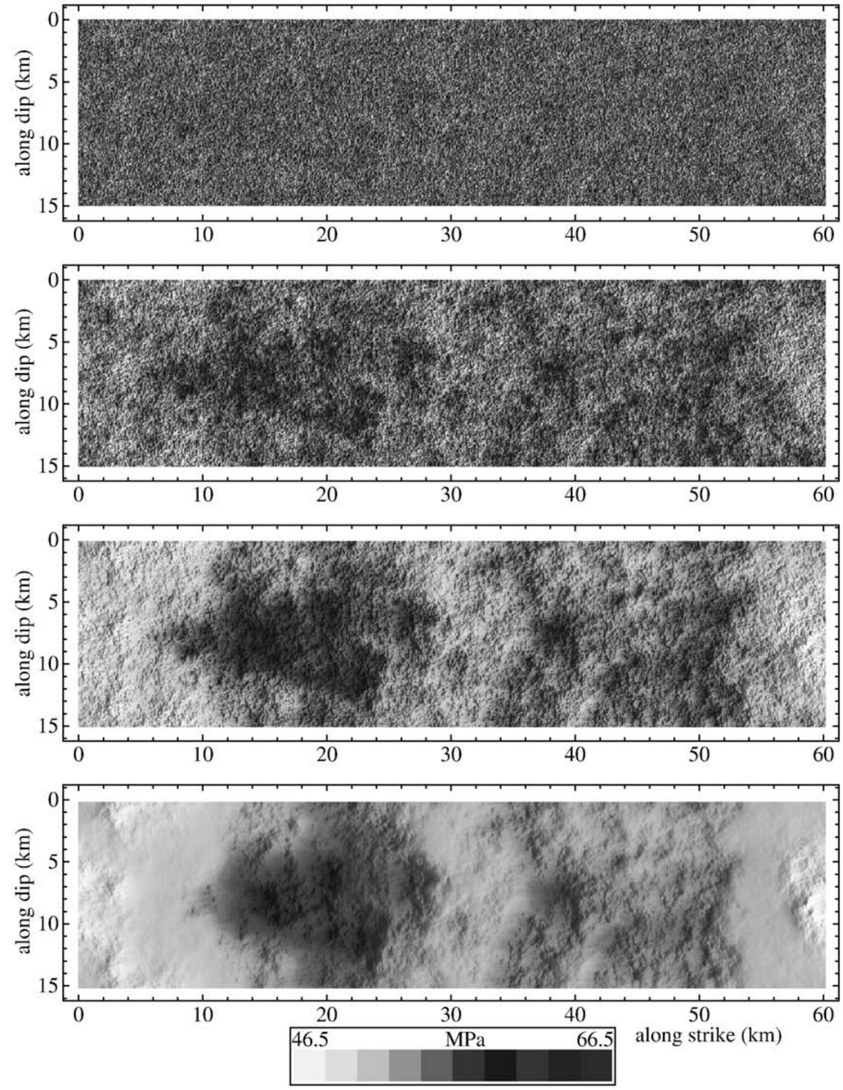

Fig. 2. Initial stress fields used for power spectral decay of $\nu=1$, 2, 3, and 4 (top to bottom). All four models were derived from the same white noise field. The model with the largest decay $\nu=4$ has the smoothest appearance. For this reason in this paper, we use the qualification "smooth" or "smoother" as a substitute for "highly correlated".

peak slip rate and rupture velocity for one of the ruptures. The rupture velocity and the peak slip rate are both less correlated (smaller ν) than the slip. In Fig. S1 in the electronic supplement we also plot the final slip distribution for the ruptures with different ν.

To compare the rupture dynamics of the four models we compute the probability density (PDF) of the source parameters within a rectangular area on the fault (Fig. 3). In Fig. 4a we compare the probability density of final slip, peak slip rate and rupture velocity over shear wave velocity for those four models.

A dependency of the source parameters on the autocorrelation of initial stress is evident. For strongly correlated stress (larger ν) the slip amplitudes and the peak slip rates are larger, and the rupture propagates faster. All this has a pronounced effect on the resulting ground motion, as discussed later.

One important feature in Fig. 4a is that the rupture with the highest correlation ($\nu=4$) has a second mode in the PDF of V_r/V_s (normalized rupture velocity) at supershear propagation speed. Because all of the models have identical κ, transition to supershear cannot be accounted for by relying only on the current definitions of κ (see Eqs. (2a) and (2b), Madariaga and Olsen, 2000; Dunham, 2007). The definition of κ should be modified to include the dependence on the parameter ν (or any other parameter measuring the effect of the spatial autocorrelation of the initial stress). The dependence can be explicit, that is, $\kappa=\kappa(S,\nu)$; or the dependence can be implicit, that is, through a parameter already included in the definition of κ (see Eqs. (2a) and (2b)). We will discuss the second alternative later. Of all the parameters included in the definition of κ, the parameter W, accounting for some characteristic fault length, such as the half width of the fault adopted in Madariaga and Olsen (2000), is the natural parameter that will be considered to include the dependence on the spatial autocorrelation (or ν) into κ. Furthermore, supershear occurs for a value of $S=1.4$ that is significantly larger than the limiting value of $S=1.19$ found by Dunham (2007) for homogeneous initial stress.

Besides the second mode occurring in the PDF of the normalized rupture velocity, there also appears a second mode in the PDF of peak slip rate for the supershear rupture ($\nu=4$). This second mode appears at lower peak slip rates. We discuss this finding in the next section.

The interdependency among different source parameters discussed in this section also illustrates the challenge of constructing a kinematic model that captures the main characteristics of dynamic rupture models (Guatteri et al., 2004; Liu et al., 2006). Fig. 4a shows that there is a dependency of the marginal distributions on the autocorrelation of stress and thus slip (Andrews, 1980). A model that has a smoother slip distribution will have on average a faster rupture velocity and larger peak slip rates. In addition, there is a spatial

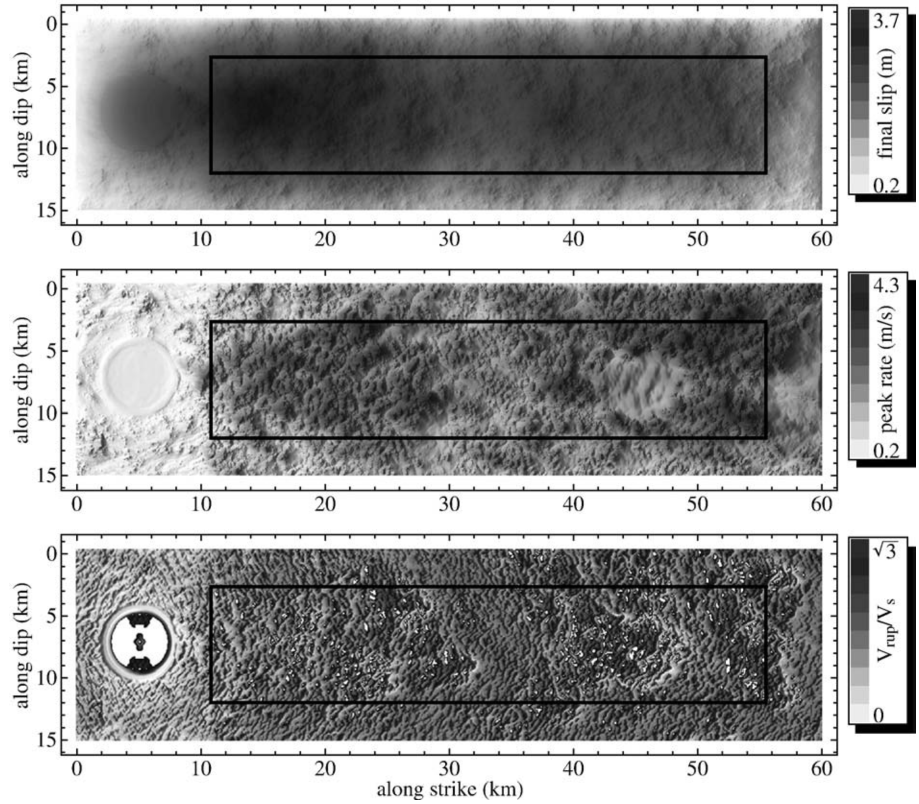

Fig. 3. Resulting final slip, peak slip rate, and rupture velocity over shear wave velocity for the model with $\nu = 2$ (subshear rupture) shown in Fig. 2. An *S*-factor of 1.4 was used to compute the strength distribution.

correlation between the parameters (Schmedes et al., 2010) that needs to be accounted for.

4.2. Fixed v, variable S-factor

In Fig. 4b we compare the PDF's of the rupture parameters for models with $v = 3$ but different *S*-factors $S = 0.8$, 1.0, 1.2, and 1.4. The PDF's for peak slip rate and the normalized rupture velocity again show two modes for the rupture models with small S. Similar to the case of homogeneous models, these models with smaller S (hence larger κ) are more likely to experience supershear propagation. The PDF of total slip shows a dependency on subshear or supershear rupture propagation as well. There is a slightly larger average total slip for the two ruptures propagating at supershear speed.

The additional mode in the PDF of peak slip rate that appears at low peak slip rates is associated with the part that of the fault that propagates at supershear speed. Lower peak slip rates for supershear rupture are discussed in detail by Bizzari and Spudich (2008); the lower peak slip rate can be expected because of a decreased singularity at the crack tip. To confirm that the modes at smaller peak slip rates correspond to supershear propagation, we separate the areas of the fault that rupture with subshear and supershear speed for one of the rupture models. We plot the PDF of peak slip rate for both cases (Fig. 5); the mode of small peak slip rates corresponds to supershear propagation. Note that in the area of the fault with supershear propagation, the peak slip rate has a minimal value 2 m/s whereas the subshear propagation has no minimum.

4.3. Variable S and variable v

Fig. 6 summarizes the results for 20 ruptures where the propagation regime (subshear or supershear) is given as a function of *S* and ν. The rupture velocity in the model that has the highest correlated stress ($\nu = 4$) goes supershear for all *S*; the rupture velocity in the model with the lowest correlation ($\nu = 1$) stays subshear for all *S* considered here. For the models with $\nu = 2$ or $\nu = 3$ the rupture goes supershear only for small *S*, as expected based on previous studies using homogeneous initial conditions (Dunham, 2007).

According to Bouchon (2008), fault geometry is one of the factors that potentially affects the transition to supershear propagation. We show that the rupture goes supershear for highly correlated stress (large value of ν); this is consistent with his observation. For a straight planar segment of a fault in a constant regional stress field we could expect that the initial stress would be almost uniform. In such a case the stress is highly correlated (compared to a fault segment with complicated geometry).

It is important to note that while supershear propagation becomes more likely as *v* increases (for a given *S*), this will not be true for $v \to \infty$. A rupture with homogeneous initial stress does not propagate at supershear speed for $S > 1.19$ (Dunham, 2007). Thus the presence of heterogeneity in the initial stress is necessary to achieve stable supershear propagation for $S > 1.19$ (also discussed by Liu and Lapusta, 2008). The role of heterogeneity in initial stress will be explained further in the section discussing the mechanism of supershear transition.

4.4. Other friction laws

Using the same stress models we computed ruptures with a time weakening law (Andrews, 2004) that ensures good resolution of the breakdown zone. One important difference between these numerical computations from those discussed earlier is the spatial dependence of the slip weakening distance. With a time weakening friction law the slip weakening distance is also heterogeneous on the fault surface. For this friction law, we also observe that supershear propagation speed is more likely for highly correlated stress (larger ν) and smaller *S*. This result is consistent with the previous observation. We find that the transition to supershear rupture speed for time weakening friction

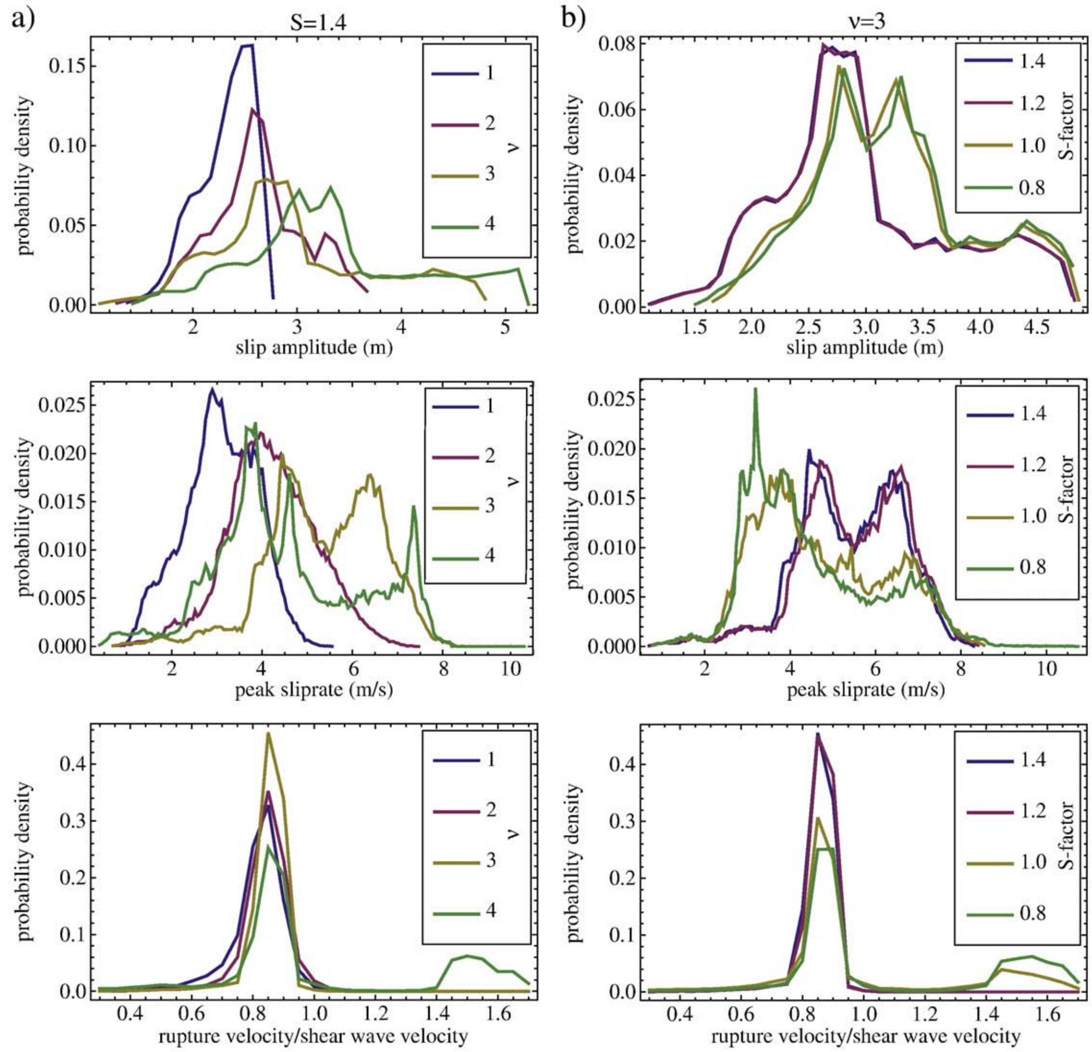

Fig. 4. a): Probability density of final slip, peak slip rate and rupture velocity over shear wave velocity for four ruptures with different power spectral decay v and $S = 1.4$. Our simulations suggest that scenarios of earthquakes with initial stress characterized by a larger value of v produce larger total slip, larger peak slip rates, and faster rupture velocities. Note that the model with the largest decay has part of the fault rupture at supershear speed. There is also a second mode of lower peak slip rates for that model corresponding to the area that propagates at supershear speeds. b) Probability density of final slip, peak slip rate and rupture velocity over shear wave velocity for four ruptures with $\nu = 3$ and different S-factor. Two models show supershear propagation and a second mode at low peak slip rates. The distinction between subshear and supershear is also visible in the PDF of final slip.

occurs for larger S and smaller values of v than for a slip weakening friction law (see Fig. S2 in electronic supplement). Compared to the simulations computed with the slip weakening friction law, the numerical results computed with a time weakening law suggest that transition to supershear velocity occurs over a larger spectrum of S and ν values.

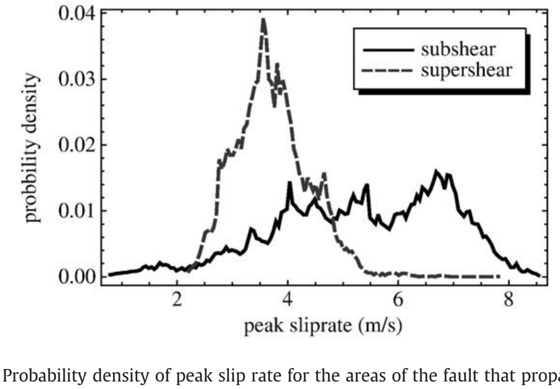

Fig. 5. Probability density of peak slip rate for the areas of the fault that propagate at subshear speed (black) and supershear speed (gray, dashed). On average supershear propagation yields smaller peak slip rates than subshear propagation. But note that there is a lower threshold of about 2 m/s for supershear propagation.

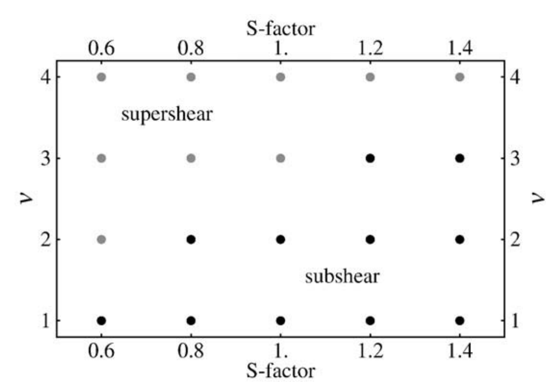

Fig. 6. Summary of the subshear or supershear propagation for the 20 ruptures as a function of S and v. For the highly correlated models (i.e., v equals 3 or 4) transition to supershear velocity is observed for a wide range of S values considered in our simulations. For the lowly correlated models (i.e., v equals 1 or 2) transition to supershear propagation is observed only for the smallest value of S or not at all.

The increased likelihood of supershear transition for a broader range of S and ν values for a time weakening friction law may have its origin in the additional spatial heterogeneity in the slip weakening distance. We computed the wavenumber spectrum of the slip weakening distance. For all models the power spectral decay ν_{dc} of the slip weakening distance is greater than the spectral decay ν of the initial stress $\nu_{dc}>\nu$, i.e., the spatial distribution of slip weakening distance is more correlated than the spatial distribution of initial stress. This might be the reason that transition to supershear speed occurs for smaller ν of initial stress (for a given S) than for the slip weakening law. For the ruptures computed using the slip weakening friction, we used constant slip weakening distance ($\nu_{dc}\rightarrow\infty$). But as shown for the initial stress, complete homogeneity decreases the likelihood of supershear transition compared to a rupture with a large but finite ν.

In addition to the slip weakening and time weakening friction laws, three dynamic ruptures are computed using a friction law based on shear transformation zone theory (Daub and Carlson, 2008; Daub et al., 2008). The initial stress is heterogeneous and the fault is embedded in a whole space. The frictional parameters are adjusted (E. Daub, pers. comm.) such that the ruptures have nearly constant S-factor, about 0.85 (see Fig. S3, electronic supplement). Supershear propagation occurs for highly correlated models (larger ν) while subshear ruptures result from the less correlated (smaller ν) models (Fig. S4 in electronic supplement). These results are qualitatively similar to the results obtained for the slip weakening friction and the time weakening friction.

The dependence of the transition to supershear velocity on the spatial heterogeneity of the initial stress (essentially controlled by the parameter ν) seems to be nearly independent of the specific formulation of the friction law.

5. Transition to supershear speed

In Fig. 7 we show snapshots in time of the stress evolution for two ruptures with different values of the correlation: $\nu=3$ and $\nu=4$. The stresses are shown for a line that is along strike through the center of the fault. In both cases, the stress propagating in front of the crack front reaches the level of strength when entering a region of low strength excess (strength minus initial stress). In this region ahead of the crack, as the stress begins to break down a daughter crack is formed. In the less correlated stress field ($\nu=3$) this daughter crack is not stable. Once the daughter crack enters a region of high strength, it vanishes and only the main crack continues propagating. In the case of a highly correlated stress field the daughter crack is stable and propagates at supershear speed, even after entering the area of high strength. For a short period of time there are two cracks propagating along the fault, but the main crack eventually vanishes resulting in a single crack propagating at supershear speed.

This situation is similar to the situations discussed by Liu and Lapusta (2008). In their model they use constant strength and simulate a crack that enters a region of high initial stress. Hence the crack also goes from an area of high strength excess to low strength excess allowing the formation of a daughter crack. One important difference is that in their model the transition would occur in a region where the slip takes large values (regions of high stress drop), whereas in our model it occurs in a region where the slip takes low values (region of low stress drop). Thus, unless we know what type of initial model discussed here–constant strength or constant S–is closer to nature, final slip cannot be used to ascertain the place on the fault where a rupture would go supershear. This is also consistent with the result that for subshear ruptures there is no correlation between final slip and local rupture velocity (Schmedes et al., 2010).

Furthermore, to achieve supershear propagation for $S>1.19$ (Dunham, 2007) requires heterogeneity in the initial stress and/or the frictional parameters. The daughter crack forms when entering a region of low strength excess after coming from a region of high strength excess. This requires heterogeneity, which is the reason why our result that supershear propagation becomes more likely for highly correlated stress cannot be extrapolated to $\nu\rightarrow\infty$, i.e., spatial homogeneous stress; and $\nu_{dc}\rightarrow\infty$, i.e., spatial homogeneous slip weakening distance.

6. Resulting ground motion

In Fig. 4a we showed that highly correlated stress (larger ν) results in larger total slip, faster rupture velocity and larger peak slip rates. Based on these results we expect a strong dependency of the resulting ground motion on the autocorrelation of initial stress. Fig. 8 shows the spatial distribution of the peak ground velocity (PGV) for the fault parallel and fault normal component on the free surface resulting from rupture scenarios produced by three initial stress states: $\nu=1$, 3 and 4, all with $S=1.4$. These ground motions correspond to the ruptures whose initial stress maps are shown in Fig. 2 and whose PDF's are shown in Fig. 4a. The first important result is that the PGV is much larger for highly correlated stress (larger ν). This is true

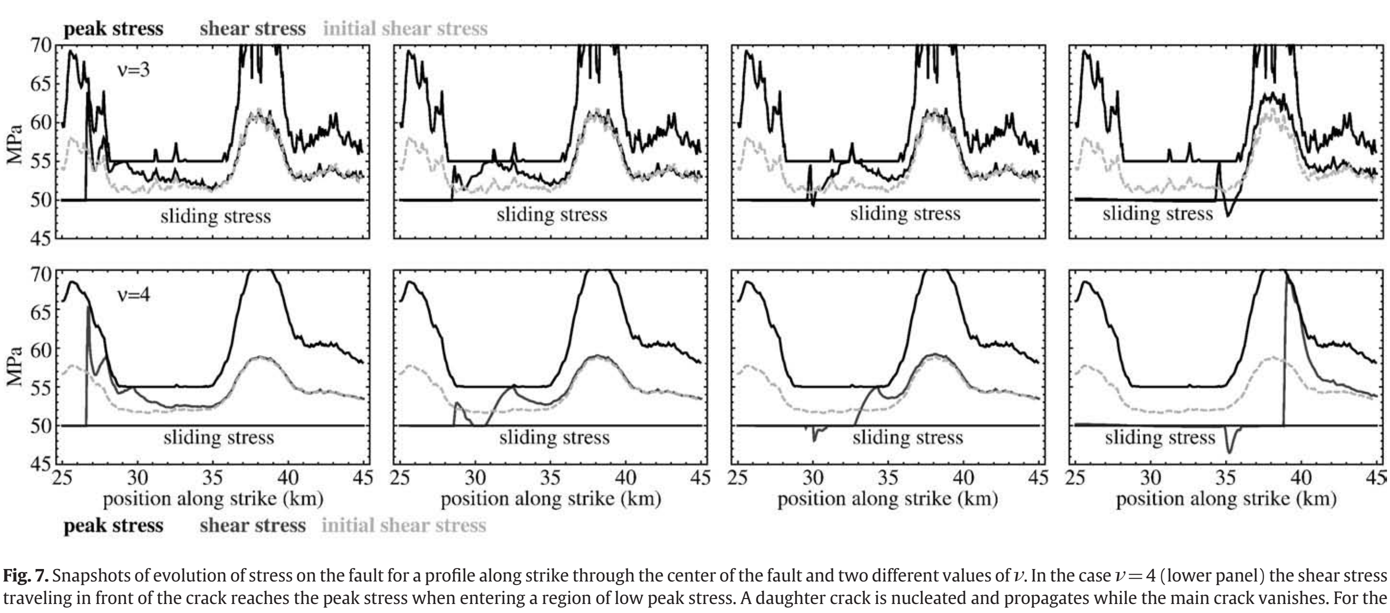

Fig. 7. Snapshots of evolution of stress on the fault for a profile along strike through the center of the fault and two different values of ν. In the case $\nu=4$ (lower panel) the shear stress traveling in front of the crack reaches the peak stress when entering a region of low peak stress. A daughter crack is nucleated and propagates while the main crack vanishes. For the model $\nu=3$ (upper panel) a daughter crack is created, but it does not become stable and vanishes while the main crack remains.

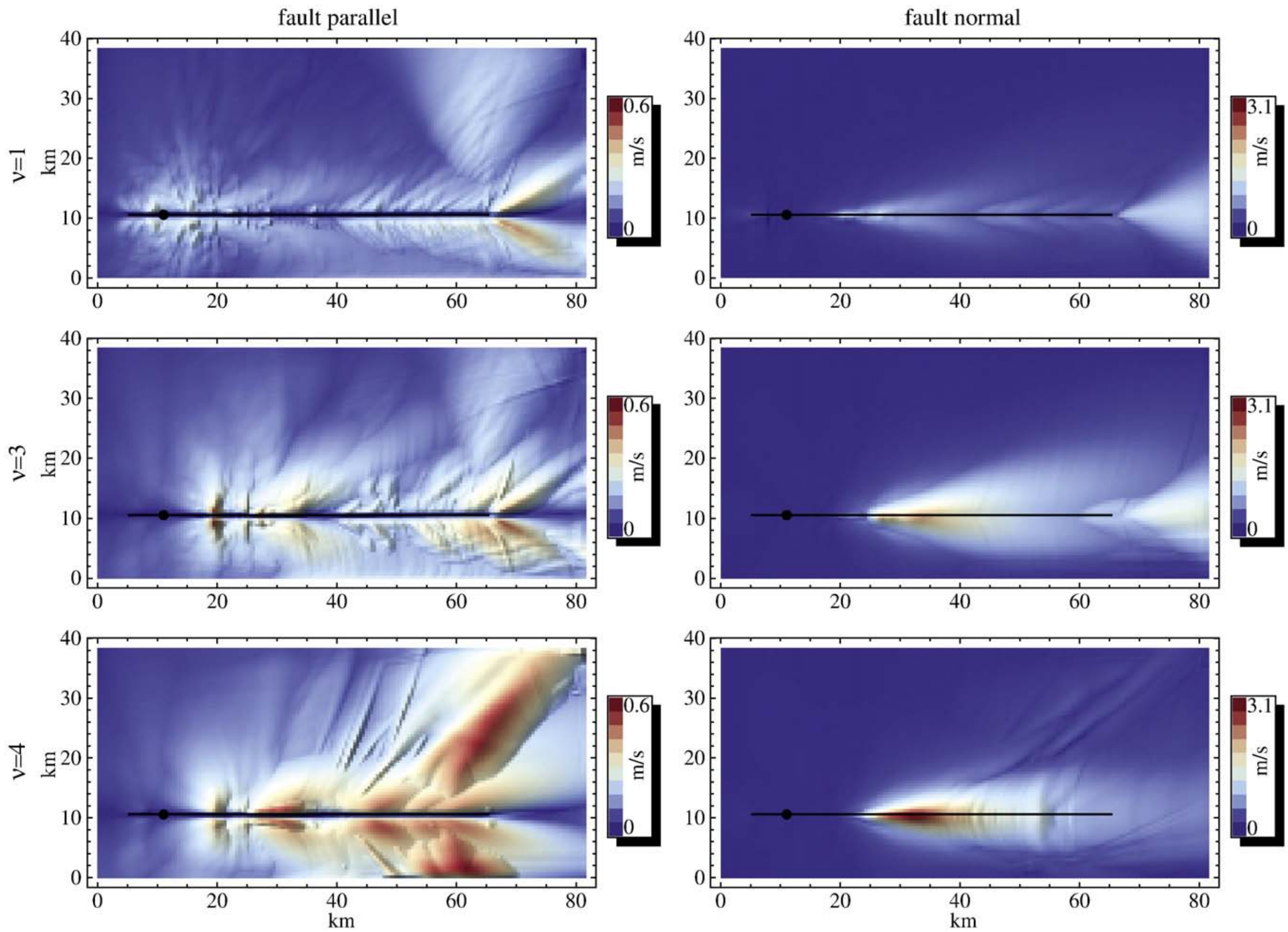

Fig. 8. Fault parallel (left) and fault normal (right) peak ground velocity for $S=1.4$ and different v. With increasing v the level of shaking increases. The rupture with the largest correlation ($\nu=4$) transitions to supershear. On the fault normal component the supershear rupture produces a PGV pattern resulting from the Mach cone (e.g., see Bernard and Baumont, 2005). On the fault normal component there is a diminished PGV behind the fault for the model $\nu=4$, i.e., no stopping phase is visible.

independently of whether the rupture propagates at subshear or supershear speed. The larger PGV is especially visible on the fault normal component. This finding is also consistent with the results discussed in Oglesby and Day (2002). They analyzed dynamic rupture models with initial heterogeneous stress and found that smooth initial stress fields produce faster ruptures and larger directivity pulses.

When comparing ground motion from ruptures that propagate at subshear and supershear speed (middle and bottom panel, respectively, in Fig. 8) one can see two distinct features: On the fault parallel component the Mach cone is clearly visible (Bernard and Baumont, 2005; Dunham and Archuleta, 2005; Dunham and Bhat, 2008; Bizzari et al., 2010). The Mach cone is responsible for large PGV occurring far from the fault when compared to scenarios characterized by ruptures propagating at subshear propagation speed. The second feature, evident on the fault normal component, is the lack of a prominent stopping phase for the supershear rupture for points located beyond the end of the fault—an observation also made by Andrews (this volume).

We can understand these observations using isochrones (Bernard and Madariaga, 1984; Spudich and Frazer, 1984). Because isochrones are the locus of points on the fault that radiate waves, which arrive at a station at the same time, one can think of isochrones as contours of arrival times. The isochrone or arrival time for a given point on the fault and a fixed observer is the time at which the rupture front reaches the point on the fault plus the time the elastic wave needs to travel from that point to the observer. Thus each observer has a different isochrone distribution because the travel times are different for different locations on the free surface. The isochrone velocity can be computed from the isochrone (arrival time) distribution in the same way as the rupture velocity is computed using the rupture times. If the isochrone contours are widely spaced, the isochrone velocity is large and elastic waves from a larger area arrive in a shorter time increment, which can produce large amplitude ground motion. If the isochrones are closely spaced, elastic waves arrive from a smaller area in a given time increment, both the isochrone velocity and the wave amplitudes are small. Directivity can be explained by large isochrone velocities (e.g. Spudich and Frazer, 1984; Schmedes and Archuleta, 2008).When an isochrone hits a barrier, like the top or the end of the fault, the isochrone becomes discontinuous and radiates a strong pulse (Bernard and Madariaga, 1984; Spudich and Frazer, 1984; Schmedes and Archuleta, 2008).

Fig. 9 plots the isochrones (arrival times) for the S-waves on the fault (middle panel) and the fault normal ground velocity (bottom panel) for a station located along strike but beyond the end of fault (top panel). For this station we compare two scenarios that have the same $\nu=3$ but different values for S: $S=1.2$ (left, subshear) and $S=1.0$ (right, supershear).

For the subshear case there is strong directivity toward the station, i.e. the isochrones are widely spaced corresponding to a large isochrone velocity. This manifests itself in a strong peak in the ground velocity between 23 and 24 s on the fault normal component, i.e. directivity. The supershear case shows no such dominant peak. Because the rupture on part of the fault travels faster than the S-wave for the supershear case, the first motion occurs a few seconds earlier than in the subshear case. Note, that in the case of supershear rupture propagation the first motion that the station experiences is not radiated from the hypocenter

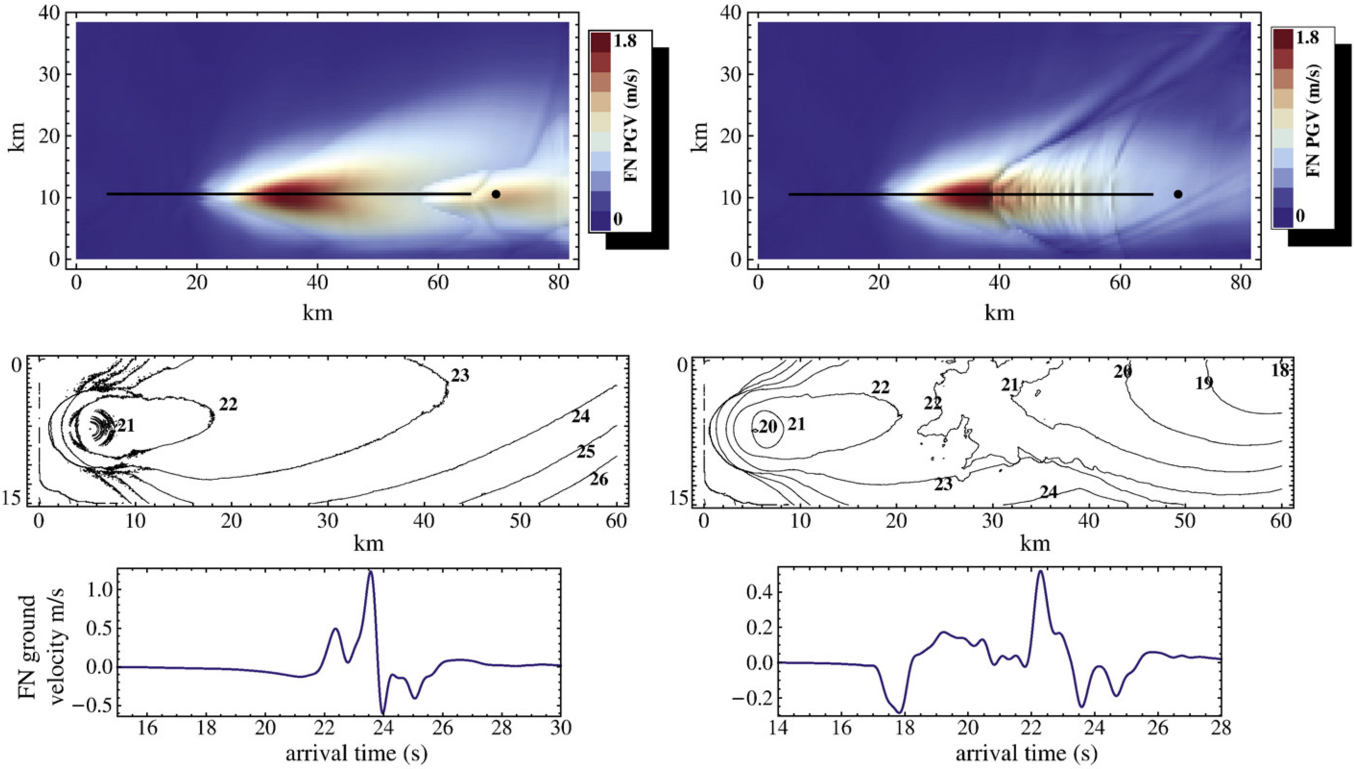

Fig. 9. Top panel shows PGV for the fault normal component and stress fields with $\nu = 3$ and $S = 1.2$ (left, subshear) and $S = 1$ (right, supershear). While the overall level of PGV is the same, the supershear rupture produces much weaker PGV beyond the end of the fault (represented by line). For the site beyond the end of the fault (black dot) the middle panel shows the arrival time contours of S-waves; the bottom panel shows the fault normal ground velocity. The duration of the record is much shorter for the subshear rupture. The isochrones for the subshear case show strong directivity resulting in a strong peak. For the supershear case the isochrone close to the station ran away from the station producing only small shaking, and the isochrones that are around the hypocenter are too far away to produce strong shaking.

but from the end of the fault. Looking at the isochrone distribution one can see that arrival times, around 18 s, correspond to radiation from the end of the fault, while the isochrones from the hypocenter indicate arrivals at about 20 s. The initial S-wave ground motion for this station is made up of isochrones arriving from the end of the fault. These isochrones are moving away from the station with a "moderate" isochrone velocity ("moderate" when compared to the subshear case that showed strong directivity); consequently this station appears to be in the back direction for directivity. This explains the lack of a stopping phase as observed in the subshear case. Isochrones coming from the beginning of the fault arrive at this station almost at the same time. However, due to the larger distance (with larger geometrical attenuation) between the hypocenter and the station, their contribution to ground motion at this station is less important. There are some peaks in the seismograms resulting from isochrones hitting the top of the fault, but again, due to the distance between these points and the station they are attenuated. When comparing the two time series– subshear and superhear ground motions – one can also see that the duration of shaking is shorter for the subshear rupture due to the large isochrone velocities, even though the total rupture duration is longer for subshear propagation. The extreme case for a station beyond the end of the fault along strike would be a rupture propagating exactly at the S-wave speed. For such a rupture this station would see the whole fault break at once (infinite isochrone velocity) yielding the maximum possible shaking.

Note, that the observation of a missing or weak stopping phase only holds when the rupture propagates at a supershear speed over a large area that is located at the end of the fault. A weak stopping phase can also result from a very heterogeneous rupture propagation. In that case only small portions of an isochrone hit the end of the fault at a given time increment producing only very small incoherent stopping phases (Schmedes and Archuleta, 2008).

Fig. 10 plots the isochrones (arrival times) for the S-waves on the fault (middle panel) and the fault parallel ground velocity (bottom panel) for a station located 12 km off the fault (top panel). This station lies in the Mach cone for the supershear rupture. We compare two scenarios with the same $\nu = 3$ but different values for S: $S = 1.2$ (left, subshear) or $S = 1.0$ (right, supershear).

For the subshear rupture there are no strong peaks in the ground velocity. There is large isochrone velocity between 20 and 22 s, but because of the distance between the station and that part of the fault as well as the radiation pattern for the fault parallel component there is no strong shaking. For the supershear rupture there is a strong pulse arriving between 19 and 20 s. Again, the isochrones reveal that there is an area of large isochrone velocity at 19–20 s that is close to the station. This area also corresponds to a larger fault parallel radiation pattern coefficient when compared to the subshear case. As in the case for a station that lies beyond the end of the fault, this station experiences shaking from waves that arrive nearly simultaneously from a region on the fault close to the station and the beginning of the fault because the rupture speed is supershear.

Another interesting feature is that if one looks at the region between the fault and the station shown in Fig. 10 there are areas that show smaller PGV even though these areas are closer to the fault. In Fig. 11 we plot in map view the fault parallel PGV. For the station 6 km off the fault we show both the P-wave and S-wave isochrones mapped onto the fault. We also show the time history of fault parallel ground velocity. This station is at the same position along strike as the station described in Fig. 10 (black dot). While closer to the fault than the station in Fig. 10, this station experiences a smaller ground velocity. For the station 12 km off the fault there is a large area of the fault surrounded by the 20 s isochrone (Fig. 10). This corresponds to a large isochrone velocity. The station 6 km off the fault has an additional isochrone in about the same area (Fig. 11), which corresponds to a

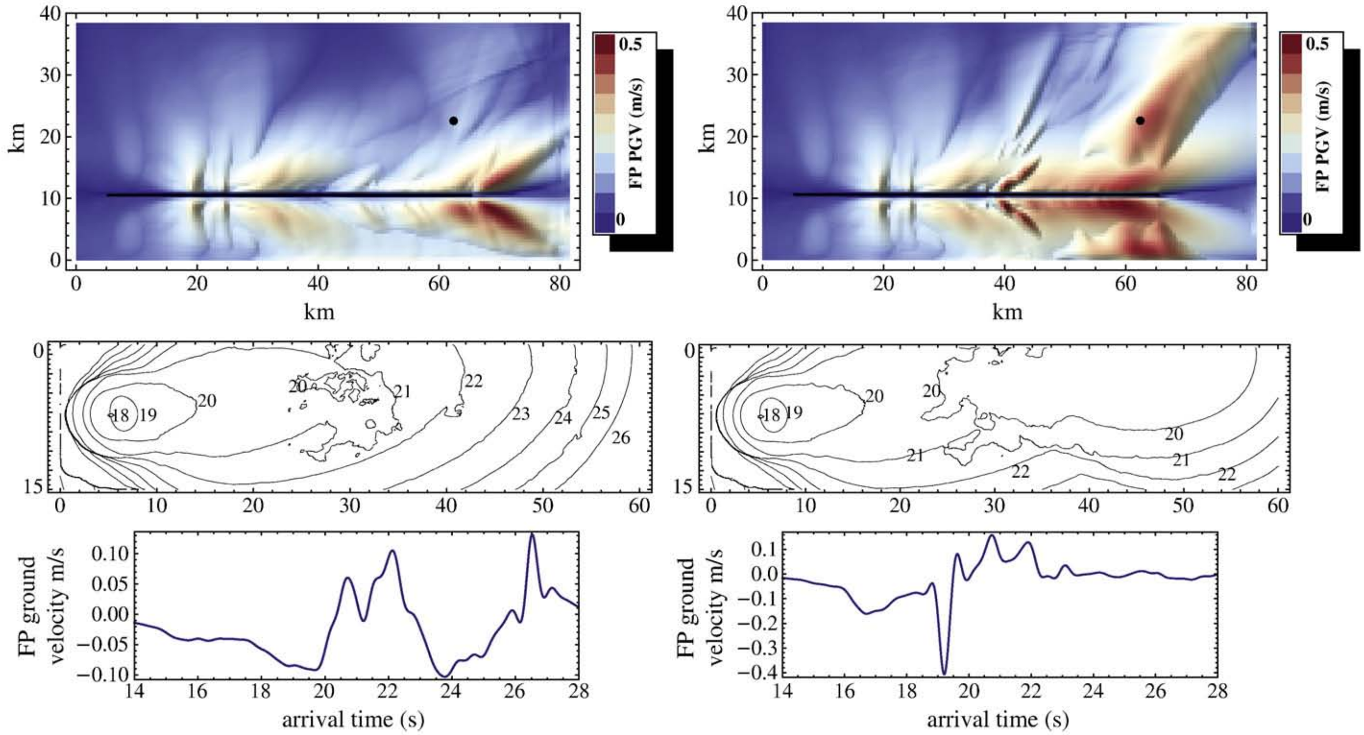

Fig. 10. Top panel shows PGV for the fault parallel component and stress fields with $\nu = 3$ and $S = 1.2$ (left, subshear) and $S = 1.0$ (right, supershear. For the site shown (black dot) the middle panel shows the arrival time contours of S-waves; the bottom panel shows the fault parallel ground velocity. The subshear case shows moderate directivity, but due to the distance of the station and the fault parallel radiation pattern no strong peak is produced. The supershear rupture produces a large isochrone velocity close to the fault that results in a strong peak even though the station is 12 km away from the fault.

smaller isochrone velocity (waves radiated from the same area arrive in a longer time span).

Note the first large peak around 16 seconds in the fault parallel ground velocity for the case with supershear propagation. This peak occurs before the first S-wave arrival; it corresponds to the P-wave. As observed and discussed by Bouchon et al. (2001), it is separated from the arrival of S-waves by a much shorter time than for subshear rupture propagation. Furthermore, it has a large amplitude that is comparable to the peak amplitude in the S-wave. Unlike S-waves the first P-wave arrival always comes from the hypocenter. But in the area where the rupture transitions to supershear, there is a large P-wave isochrone velocity; this results in the large P-wave peak on the fault parallel component. Hence, besides the Mach cone visible in the fault parallel PGV one can also expect to see stronger directivity in ground motion generated by the P-waves for supershear ruptures.

The position of the station 6 km off the fault is similar to the position of the El Centro stations close to the fault for the 1979 Imperial Valley earthquake (Archuleta, 1982). Archuleta (1984) proposes that the rupture is subshear in the first part of the fault and then propagates at supershear speed for about 15 km. The station 6 km off the fault that experiences strong P-wave directivity for the supershear rupture (Fig. 11) also experiences shaking resulting from a rupture that is first subshear and then transitions to supershear. Archuleta (1982) and Spudich and Cranswick (1984) discuss large vertical accelerations that arrive before the first S-wave arrival at the stations at the El Centro array close to the fault. These might be explained by P-wave directivity discussed above (see Fig. 11). In Fig. S5 (electronic supplement) we plot the vertical acceleration and velocity for this station 6 km off the fault for a subshear and a supershear rupture. For comparison the vertical velocity and acceleration recorded at station E08 (low passed to 5 Hz) during the Imperial Valley earthquake are shown as well. The synthetic supershear rupture produces a large vertical acceleration that arrives before the first S-wave arrival. Furthermore, velocity and acceleration both show two large pulses, as also observed for E08, while the subshear case only shows one pulse. Hence the supershear rupture process proposed by Archuleta (1984) is a possible explanation for the observed large vertical accelerations.

7. A modified dimensionless parameter to describe supershear transition

We have shown in the previous sections that the rupture propagation is strongly dependent on the power spectral decay, or more generally, the autocorrelation of initial stress. In this section we introduce a dimensionless parameter that keeps the simplicity of the parameter κ (Eqs. (2a) and (2b)) introduced by Madariaga and Olsen (2000) while being general enough to account for heterogeneity in the initial stress.

For heterogeneous stress models, we define a κ_{ac} where the subscript ac stands for autocorrelation. To take into account the heterogeneity, we introduce a new length scale W_{ac} that depends on the power spectrum of the initial stress. We define

$$\kappa_{ac} = \frac{\langle \tau_0 - \tau_d \rangle^2 W_{ac}}{\langle \mu \rangle \langle \tau_p - \tau_d \rangle \langle d_c \rangle} \qquad (3)$$

Here $\langle x \rangle$ denotes the mean value of the parameter x over the whole fault plane. The definition of κ_{ac} mainly differs from the original description (Eqs. (2a) and (2b)) because of W_{ac}, and the use of the mean value for the other parameters. The following derivation applies for any shape of the power spectrum, not only power laws.

First, we compute the average 1D power spectrum as the average of the 1D power spectra for all profiles along dip, i.e., for all profiles with constant position along strike. We will explain the reason for this choice after the following derivations.

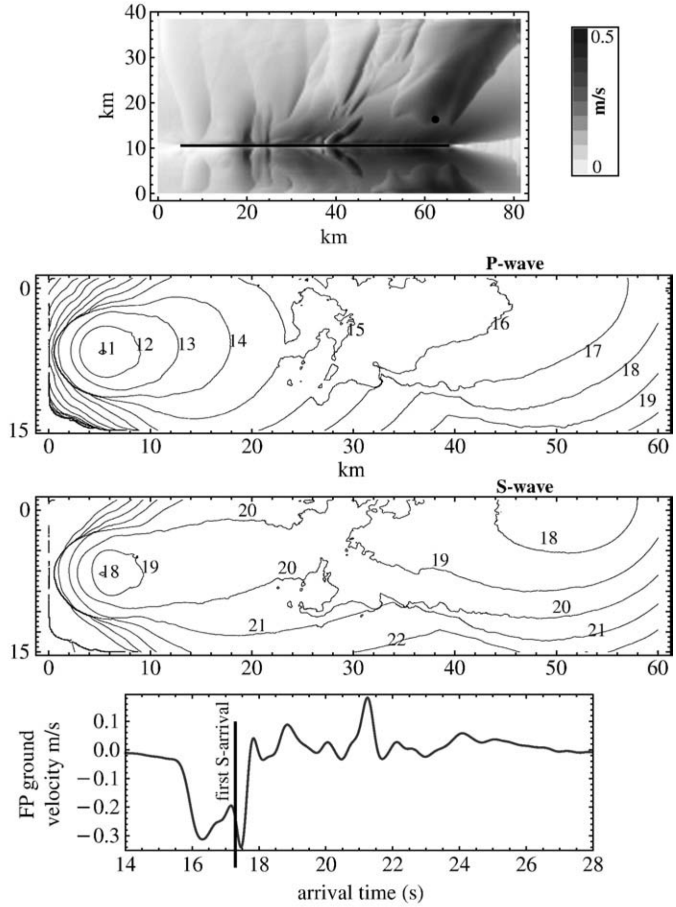

Fig. 11. Top panel shows fault parallel PGV in map view for supershear rupture with $S=1$ and $\nu=3$, see also Fig. 10. Black dot indicates the position of station which is about 6 km off the fault. It experiences weaker shaking than a station 12 km off the fault (Fig. 10). Two middle panels show P-wave and S-wave isochrones. Bottom plot shows fault parallel ground motion at the station. The first strong peak is from a large P-wave isochrone velocity around 16 seconds in the area that ruptures supershear; this peak is the result of P-wave directivity. The S-wave motion is weaker than for the station in Fig. 10 because there is a lower isochrone velocity for the station shown here.

Let p_i be the average power spectral density corresponding to the wavenumber k_i. Then the weight ψ_i is defined as

$$\psi_i = p_i / \sum_j p_j \tag{4}$$

with the property $\sum \psi_i = 1$. The ψ_i are independent of the convention used for the Fourier transform because any factor (like 2π) cancels out. We define $l_i = 2\pi/k_i$ as the length scale (or wavelength) associated with the wavenumber k_i. We compute the length scale W_{ac} as the weighted sum of the length scales l_i. The weights are derived from the shape of the power spectrum, as discussed above.

$$W_{ac} = \sum \psi_i l_i \tag{5}$$

Note, that in all computations the zero wavenumber is excluded because it would lead to an infinite length scale.

For the four stress fields shown in Fig. 2 with $\nu = 1, 2, 3,$ and 4, the computed W_{ac} takes the values 1931 m, 6043 m, 12,122 m, 13,373 m, respectively. The highly correlated model ($\nu=4$) has a larger W_{ac} because it has lower weights at the high wavenumbers (small length scales). Hence the parameter W_{ac} shows the expected dependence on the autocorrelation of initial stress because κ_{ac} increases with the power spectral decay ν.

Note, that alternative derivations of W_{ac} are possible. For instance, an alternative formulation consists in performing the weighted sum of the wavenumbers, e.g. $\mathbb{W}_{ac} = 2\pi/\Sigma\Psi_i k_i$. This yields a different range of values but the same relative behavior (larger value for higher correlated stress field).

We chose profiles that are taken along dip (profiles of constant position along strike) to compute W_{ac} for two reasons. First, the width of the fault determines the average arrival time of the healing phases, which can prevent the daughter crack from becoming stable, i.e., no supershear propagation. Dunham (2007) discusses the influence of fault width on the occurrence of supershear. However, one might argue that for a longer fault there is a higher probability for supershear rupture to occur because it is more likely to find a region of high strength excess followed by low strength excess. By using profiles along strike (profiles of constant position along dip) one would account for this by getting a larger W_{ac} for a longer fault. The problem with such a formulation of W_{ac} is that even for a very rough stress model for which supershear propagation can never be achieved, one can get a large W_{ac} if the fault is long enough and hence a large κ_{ac}. To avoid a dependence on the length of the fault, we chose profiles along dip (constant position along strike).

7.1. Application to 300 dynamic rupture simulations

To validate the parameter κ_{ac} we use more than 300 dynamic ruptures discussed in Schmedes et al., (2010). These ruptures provide a relevant test set for the following reasons: (i) There is a large number of scenarios of ruptures in the set. (ii) The set includes ruptures that propagate at subshear speed and ruptures that propagate at supershear speeds. (iii) It includes ruptures computed under different conditions. For instance, the spectrum of the initial stress is either described by a power law function (Andrews, 1980; Lavallée and Archuleta, 2003; Liu-Zeng et al., 2005) or the von Karman function (Sommerville et al., 1999; Mai and Beroza, 2002; Guatteri et al., 2003; Liu et al., 2006). Subsets of scenarios also differ by the approaches used to compute the shear strength and the slip weakening distance, both of which can be constant or heterogeneous over the fault plane. For the rupture with heterogeneous shear strength it also includes ruptures which have a variable S. In addition to the ruptures computed by Schmedes et al., (2010), the data base contains six 300 km long ruptures for a fault embedded within a 3D velocity structure for southern California (Dalguer et al., 2008; Olsen et al., 2009). For ruptures with heterogeneous friction parameters (such as strength or slip weakening distance) the autocorrelation of the frictional parameters is the same as for the initial stress.

We compute κ_{ac} for all (>300) ruptures that used a linear slip weakening friction law. As a measure of supershear propagation, we compute the fraction of the fault area that propagates above the Eshelby speed $\sqrt{2}V_S$. In Fig. 12a we plot the fraction of the fault above the Eshelby speed versus κ_{ac}. We colored coded different models of initial stress. The larger dots correspond to the six 300 km long ruptures embedded in a 3D velocity model. In general, there is a clear boundary defined by the critical number $\kappa_{ac}^{(c)} \approx 1$ below which there is no rupture that propagates at supershear speed. For values $\kappa_{ac} > \kappa_{ac}^{(c)}$ there is a mixed regime of ruptures that propagate either subshear or supershear.

These results suggest that for $\kappa_{ac} > 1$ there exists a finite probability that the rupture transitions to supershear propagation. This is a different result from the one obtained for homogeneous ruptures discussed in Madariaga and Olsen (2000). In Madariaga and Olsen (2000), the rupture remains at subshear speed for all κ smaller than a critical value, while for all κ larger than a critical value the rupture transitions to supershear speed. In their framework, there are two regimes of propagation completely determined by a single critical value $\kappa^{(c)}$. The results summarized in Fig. 12a indicate that for κ_{ac} values smaller than the critical value $\kappa_{ac}^{(c)}$ the rupture remains at

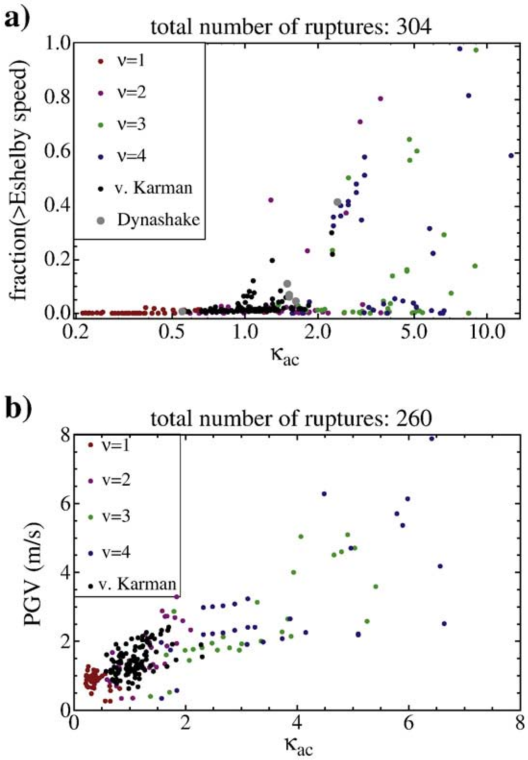

Fig 12. a): κ_{ac} versus the fraction of the fault that propagates above the Eshelby speed. Color coding is assigned according to different autocorrelation of initial stress. Dynashake corresponds to the six 300 km long ruptures embedded in a 3D velocity model (Dalguer et al., 2008; Olsen et al., 2009). No supershear propagation is observed for $\kappa_{ac}<1$ in all cases. All ruptures with a power spectral decay of 1.0 stay subshear. b) κ_{ac} versus the maximum PGV found anywhere on the free surface. Color coding is assigned according to autocorrelation of initial stress. While decays of $\nu=1$, 2 and von Karman yield PGV's in the range of those recorded for past earthquakes, the rupture models with power spectral decay $\nu=3$, 4 yield much larger PGV values.

subshear speed (as predicted in Madariaga and Olsen, 2000 but for a different definition of κ than given in Eqs. (2a) and (2b)). However, when the value of κ_{ac} exceeds $\kappa_{ac}{}^{(c)}$, transition to supershear is observed only for a subset of scenarios with $\kappa_{ac}>\kappa_{ac}^{(c)}$. This suggests that while there is a finite probability for a transition to supershear velocity when $\kappa_{ac}>\kappa_{ac}^{(c)}$, it is not a certainty. Thus $\kappa_{ac}>\kappa_{ac}^{(c)}$ is a necessary condition for the occurrence of supershear rupture propagation, but not a sufficient one. Other factors, like the length of the fault, may play a significant role in the transition to supershear velocity. But the length of the fault is only important for ruptures that have an autocorrelation that allows supershear rupture propagation. A long fault does not increase the likelihood of supershear transition for faults with an initial stress field that is weakly correlated.

Consider a scenario where the initial conditions are such that $\kappa_{ac}>\kappa_{ac}^{(c)}$. In this scenario there is a probability larger than zero for finding an area on the fault that favors a transition to supershear. However, by shifting the location of the hypocenter toward or away from such a favorable area we modify the distance the rupture travels until it reaches this favorable area. This will result in a different rupture velocity when reaching the favorable area (Schmedes et al., 2010) and thus affect the transition to supershear propagation. Hence, for heterogeneous ruptures a single dimensionless parameter is probably not sufficient to predict with certainty the transition to supershear velocity.

A similar conclusion was drawn for the Reynolds number in fluid mechanics. In fluid mechanics, it was first postulated that increasing the Reynolds number R of a fluid above a critical value would lead to a transition from a stable laminar flow to an unstable turbulent flow. The Reynolds number is a dimensionless number obtained by combining a characteristic length, a characteristic (or average) velocity and the dynamic viscosity of the fluid. This theory turned out to be inadequate since it was observed that if a flow were stable for Reynolds numbers smaller than a critical value R_{inf} the flow may or may not remain stable for Reynolds numbers exceeding R_{inf}. Other factors such as the surface roughness of the solid in contact with fluid have to be considered (Landau and Lifshitz, 1987). In analogy with our understanding of the transition to turbulence in fluid mechanics, understanding and quantification of the transition to supershear during an earthquake may require more than one single dimensionless number.

In our case, one thus can only state that for multiple ruptures with a $\kappa_{ac}>\kappa_{ac}^{(c)}$ there is a likelihood that subset will transition to supershear propagation speeds. This also means that Fig. 6 is strictly valid only for the set of ruptures we computed. The general result that larger ν is more likely to produce supershear propagation holds true. But for a given S and ν, a different stress field or a different position of the hypocenter might result in either subshear or supershear rupture if $\kappa_{ac}\geq 1$.

In contrast, for $\kappa_{ac}<1$ our results suggest that rupture propagation is always subshear. Of course due to the finite number of scenarios there might be supershear ruptures that were not sampled with our data set. Thus we can only assume that for $\kappa_{ac}<\kappa_{ac}^{(c)}$ the probability is 0 or close to 0 for supershear rupture propagation.

Fig. 12a also illustrates the dependence of supershear propagation on the autocorrelation of initial stress. All ruptures that have $\nu=1$ (a total of 56) stay subshear. This is also captured by the values of κ_{ac} which are smaller than 1.0 for all but one rupture, which has a value only slightly above 1.0. Ruptures with $\nu=2$ have κ_{ac} below and above 1.0 and show both subshear and supershear propagation. Ruptures with $\nu=3$ or 4 always yield $\kappa_{ac}>1$; they produce both subshear and supershear propagation.

Note that, as indicated earlier, for ruptures that have heterogeneous friction parameters it is important to take their autocorrelation into account. In all ruptures computed using the slip weakening law, we used the same power spectral decay for the frictional parameters as for the initial stress. But when we used a time weakening friction law, we observed that a transition to supershear propagation speed is more likely than for the slip weakening law. The probable reason is that the resulting slip weakening distance is more correlated than the initial stress, meaning $W_{ac}(d_c)>W_{ac}(\tau_0)$. One way to incorporate length scales of frictional parameters that are different from the initial stress would be to use the mean of the length scales involved, e.g., for the rupture computed using the time weakening friction law one would use $(W_{ac}(d_c)+W(\tau_0))/2$ as length scale in the definition of κ_{ac}. Fig. S6 in the electronic supplement shows the fraction of the fault above the Eshelby speed versus the parameter $\overline{\kappa_{ac}}=(\kappa_{ac}(\tau_0)+\kappa_{ac}(d_c))/2$ incorporating the autocorrelation of initial stress as well as slip weakening distance. Again, there is a no supershear rupture for a value of about $\overline{\kappa_{ac}}<1$.

7.2. Influence of κ_{ac} on ground motion

The basic parameters that define κ_{ac} will all have some effect on ground motion. For instance, we expect larger ground motion for smaller S, or larger ratios of $(\tau_o-\tau_d)/\mu$. As shown in Fig. 8, the ground motion amplitude is larger for highly correlated initial stress, i.e., larger W_{ac}.

In Fig. 12b we plot κ_{ac} versus the largest peak ground velocity (PGV) on the free surface for different autocorrelations of stress. We use 260 dynamic ruptures computed in a half space. There is a clear positive correlation between the PGV and κ_{ac}. Of course, the peak ground motion depends on many other factors, such as site response or seismic attenuation. However, for two faults embedded within the same velocity model κ_{ac} provides a straightforward way to estimate which model produces larger peak ground motion.

From Fig. 12b one can also see how different maximal PGV's are related to different autocorrelations of stress. The stress fields with $\nu=1$ and 2, and the stress derived from von-Karman slip maps (Sommerville et al., 1999; Mai and Beroza, 2002; Guatteri et al., 2003; Liu et al., 2006) yield values that are in the range of what has been observed to date . In contrast, the rupture models with $\nu=3$ and 4 produce PGV's much larger than have been observed to date (Shin et al., 2000). This is consistent with the observation (Fig. 4a) that a smoother initial stress yields larger slip, faster rupture velocities and larger peak slip rates.

The extreme PGV's shown in Fig. 12b occur right at the fault trace. Because observations in the near field of large strike slip earthquakes are sparse, we might not have recorded such extreme PGV's. Another caveat is that the dynamic models are computed in a half space with constant normal stress. But given that the models with $\nu=3$ and 4 produce much larger PGV's than the maximums observed, one could speculate that the autocorrelation of stress in the Earth is in the range of $\nu=1$ or 2 for most earthquakes.

8. Conclusions

Using a large suite of dynamic rupture models we find that transition to supershear rupture propagation is more likely to occur for faults (or fault segments) that have a large autocorrelation in initial stress, i.e., for faults where the spatial distribution of initial stress appears smooth (see Fig. 2). This is in good agreement with the observation by Bouchon (2008) that supershear ruptures tend to occur on simple geometries for which we expect almost uniform, i.e., highly correlated, stress conditions.

We find that the transition to supershear propagation speed occurs when the rupture enters from a region of high strength excess into a region of low strength excess thereby enabling the formation of a daughter crack. Either a region of high pre-stress and constant strength or a region of low pre-stress and low strength can create this circumstance. The important difference is that in the former the transition occurs in areas that will have large total slip while in the latter these areas will have small total slip. Hence, total slip is not a useful parameter to predict where a transition to supershear propagation might occur in a kinematic framework (see also Schmedes et al., 2010).

The transition to supershear speed is influenced not only by the spatial distribution of initial stress but also by the spatial distribution of the slip weakening distance. With a time weakening friction law the slip weakening distances have a greater spatial correlation than the initial stress. In this situation we find a greater likelihood for a transition to supershear speed for a given S and ν.

Besides facilitating the transition to supershear rupture propagation the autocorrelation of stress greatly influences the rupture dynamics and ground motion for both subshear and supershear rupture. A fault that has a smooth initial stress shows larger maximal slip, larger peak slip rates, and faster rupture velocity (see Fig. 4a and b). As a consequence, highly correlated models produce larger ground motion. For ruptures that propagate at supershear speeds we find certain characteristics that are different from subshear ruptures. Parts of the fault that rupture at supershear speed have, on average, lower peak slip rates than parts that propagate at subshear speed confirming the results in Bizzari and Spudich (2008).

Because of the Mach cone large ground motion appears on the fault parallel component at distances far from fault as noted by Dunham and Archuleta (2005) and Dunham and Bhat (2008). We also observe that the stopping phase is absent or diminished. For a station that lies beyond the end of the fault the first motion originates from the end of the fault that is closer to the station; all the subsequent isochrones are moving away from the station yielding small ground motion as if the station were in the back azimuth of the rupture. Diminished stopping phases can also be produced by very heterogeneous rupture propagation that would produce very irregular isochrones (Schmedes and Archuleta, 2008).

While directivity effects for S-waves are not an issue for supershear propagation, directivity effects for ground motion generated by P-waves come to the forefront. This strong P-wave directivity offers a possible explanation for the large vertical accelerations observed during the 1979 Imperial Valley earthquake (Archuleta, 1982; Spudich and Cranswick, 1984). Bizzari et al. (2010) find an elevated spectral acceleration at high frequencies for a few of the Imperial Valley stations close to the fault, which is consistent with their finding that stations experiencing mach pulses should be richer in high frequencies. Interestingly, among all events they analyzed, the Imperial Valley earthquake is the only event, for which they could observe an elevated spectral acceleration at high frequencies.

In general, it is important to consider the possibility of supershear ruptures for hazard assessment because the spatial distribution of ground motion is so different from that generated by subshear ruptures. In particular, large amplitude ground motions can extend farther from the fault and the polarization of the maximum ground motion is completely different—fault parallel rather than fault normal.

Based on the original definition of κ by Madariaga and Olsen (2000) we introduced a modified parameter κ_{ac} that incorporates a characteristic length scale W_{ac}, which depends on the autocorrelation of the initial stress field. For κ_{ac} smaller than the critical value $\kappa_{ac}^{(c)}$, the rupture propagates at subshear speed (as predicted in Madariaga and Olsen, 2000 but for a different definition of the parameter κ given in Eqs. (2a) and (2b)). However, when κ_{ac} exceeds $\kappa_{ac}{}^{(c)}$, transition to supershear is observed only for a subset of scenarios with $\kappa_{ac}>\kappa_{ac}^{(c)}$. Thus when $\kappa_{ac}>\kappa_{ac}^{(c)}$ there is a probability for a transition to supershear velocity but not a certainty. This is different from the theory advanced in Madariaga and Olsen (2000) where a transition to supershear velocity is uniquely constrained by κ exceeding a critical value.

The parameter κ_{ac} also correlates well with the computed PGV at the free surface. As such κ_{ac} could be used to predict which scenarios of dynamic ruptures are likely to yield larger ground motion without actually computing a dynamic rupture.

We also find, that ruptures with a high degree of correlation in initials stress, $\nu=3$ and $\nu=4$, produce PGV values significantly larger than the largest observed PGV to date. Furthermore, for values $\nu=3$ and $\nu=4$ we always find that $\kappa_{ac}>\kappa_{ac}^{(c)}$. This would imply that supershear propagation should occur often in nature if the stress were highly correlated. If we assume that supershear ruptures don't occur very often, this would imply that the stress in the Earth is less correlated implying a smaller ν in the range of 1 and 2 for strike slip faults, corresponding to a Fourier spectral decay of slip that is −1.5 and −2, respectively (see also Lavallée et al., 2006).

Acknowledgements

We thank Eric Daub for providing us with the three rupture models discussed and Luis Dalguer for providing the DynaShake parameters from the six, 300 km long ruptures. We thank two anonymous reviewers for valuable and helpful comments. This research was supported by the Southern California Earthquake Center (SCEC) and by UCSB matching funds to SCEC. SCEC is funded by NSF Cooperative Agreement EAR-0106924 and USGS Cooperative Agreement 02HQAG0008. We have also received support through a gift from Pacific Gas and Electric to the Institute for Crustal Studies (ICS). This is SCEC contribution number 1423. This material is also based upon work supported by the National Science Foundation under grant 0738954. This is ICS contribution No. 1010.

Appendix A. Supplementary data

Supplementary data associated with this article can be found, in the online version, at doi:10.1016/j.tecto.2010.05.013.

References

Aagaard, B.T., Heaton, T.H., 2004. Near-source ground motions from simulations of sustained intersonic and supersonic fault ruptures. Bull. Seismol. Soc. Am. 94 (6), 2064–2078.

Andrews, D.J., 1976. Rupture velocity of plane strain shear cracks. J. Geophys. Res. 81.

Andrews, D.J., 1980. A stochastic fault model: I. Static case. J. Geophys. Res. 85, 3867–3877.

Andrews, D.J., 2004. Rupture models with dynamically determined breakdown displacement. Bull. Seismol. Soc. Am. 94 (3), 769–775.

Archuleta, R.J., 1982. Analysis of near-source static and dynamic measurements from the 1979 Imperial Valley earthquake. Bull. Seismol. Soc. Am. 72 (6A), 1927–1956.

Archuleta, R.J., 1984. A faulting model for the 1979 Imperial Valley earthquake. J. Geophys. Res. 89, 4559–4585.

Bernard, P., Baumont, D., 2005. Shear mach wave characterization for kinematic fault rupture models with constant supershear rupture velocity. Geophys. J. Int. 162 (2), 431–447.

Bernard, P., Madariaga, R., 1984. A new asymptotic method for the modeling of near-field accelerograms. Bull. Seismol. Soc. Am. 74 (2), 539–557.

Bhat, H.S., Dmowska, R., King, G.C.P., Klinger, Y., Rice, J.R., 2007. Off-fault damage patterns due to supershear ruptures with application to the 2001 mw 8.1 Kokoxili (Kunlun) Tibet earthquake. J. Geophys. Res. 112.

Bizzari, A., Spudich, P., 2008. Effects of supershear rupture speed on the high-frequency content of S waves investigated using spontaneous dynamic rupture models and isochrone theory. EOS 89 (53).

Bizzari, A., Dunham, E.M., Spudich, P., 2010. Coherence of mach fronts during heterogeneous supershear earthquake rupture propagation: simulations and comparison with observations. JGR 115 (B08301).

Bouchon, M., 2008. Some characteristics of supershear ruptures. EOS 89 (53, Suppl), S43E-04.

Bouchon, M., Karabulut, H., 2008. The aftershock signature of supershear earthquakes. Science 320 (5881), 1323–1325.

Bouchon, M., Vallée, M., 2003. Observation of long supershear rupture during the magnitude 8.1 Kunlunshan earthquake. Science 301 (5634), 824–826.

Bouchon, M., Bouin, M.-P., Karabulut, H., Nafi, T., Dietrich, M., Rosakis, A.J., 2001. How fast is rupture during an earthquake ? New insights from the 1999 Turkey earthquakes. Geophys. Res. Lett., 28.

Burridge, R., 1973. Admissible speeds for plane-strain self-similar shear cracks with friction but lacking cohesion. Geophys. J. R. Astron. Soc. 35 (4), 439–455.

Campillo, M., Favreau, P., Ionescu, I.R., Voisin, C., 2001. On the effective friction law of a heterogeneous fault. J. Geophys. Res. 106 (B8), 16,307–16,322.

Dalguer, L.A., Day, S.M., Olsen, K.B., Cruz-Atienza, V.M., 2008. Rupture models and ground motion for shakeout and other southern san andreas fault scenarios. CD of 14th World Conference on Earthquake Engineering, Int. Assoc. for Earthquake Eng., Beijing, China.

Das, S., Aki, K., 1977. A numerical study of two-dimensional spontaneous rupture propagation. Geophys. J. R. Astron. Soc. 50 (3), 643–668.

Daub, E.G., Carlson, J.M., 2008. A constitutive model for fault gouge deformation in dynamic rupture simulations. J. Geophys. Res. 113.

Daub, E.G., Manning, M.L., Carlson, J.M., 2008. Shear strain localization in elastodynamic rupture simulations. Geophys. Res. Lett. 35.

Day, S.M., 1982. Three-dimensional simulation of spontaneous rupture: the effect of nonuniform prestress. Bull. Seismol. Soc. Am. 72 (6A), 1881–1902.

Dunham, E.M., 2007. Conditions governing the occurrence of supershear ruptures under slip-weakening friction. J. Geophys. Res. 112 (B07302).

Dunham, E.M., Archuleta, R.J., 2004. Evidence for a supershear transient during the 2002 denali fault earthquake. Bull. Seismol. Soc. Am. 94 (6B), S256–268.

Dunham, E.M., Archuleta, R.J., 2005. Near-source ground motion from steady state dynamic rupture pulses. Geophys. Res. Lett. 32 (L03302).

Dunham, E.M., Bhat, H.S., 2008. Attenuation of radiated ground motion and stresses from three-dimensional supershear ruptures. J. Geophys. Res. 113.

Dunham, E.M., Favreau, P., Carlson, J.M., 2003. A supershear transition mechanism for cracks. Science 299 (5612), 1557–1559.

Ellsworth, W.L., et al., 2004. Near-field ground motion of the 2002 Denali Fault, Alaska, earthquake recorded at pump station 10. Earthq. Spectra 20 (3), 597–615.

Freund, L.B., 1979. The mechanics of dynamic shear crack propagation. J. Geophys. Res. 84.

Guatteri, M., Mai, P.M., Beroza, G.C., Boatwright, J., 2003. Strong ground-motion prediction from stochastic-dynamic source models. Bull. Seismol. Soc. Am. 93 (1), 301–313.

Guatteri, M., Mai, P.M., Beroza, G.C., 2004. A pseudo-dynamic approximation to dynamic rupture models for strong ground motion prediction. Bull. Seismol. Soc. Am. 94 (6), 2051–2063.

Ida, Y., 1972. Cohesive force across the tip of a longitudinal-shear crack and Griffith's specific surface energy. J. Geophys. Res. 77 (20), 3796–3805.

Johnson, T., Wu, F.T., Scholz, C.H., 1973. Source parameters for stick-slip and for earthquakes. Science 179, 278–280.

Kaneko, Y., Lapusta, N., Ampuero, J.P., 2008. Spectral element modeling of spontaneous earthquake rupture on rate and state faults: effect of velocity-strengthening friction at shallow depths. J. Geophys. Res. 113, B09317. doi:10.1029/2007JB005553.

Landau, L.D., Lifshitz, E.M., 1987. Fluid Mechanics. Butterworth-Heinemann, Oxford.

Lavallée, D., 2008. On the random nature of earthquake sources and ground motions. In Earth Heterogeneity and Scattering Effects in Seismic waves, Advances in Geophysics, 50. [Jan, you need to give the publisher.]

Lavallée, D., Archuleta, R., 2003. Stochastic modeling of slip spatial complexities for the 1979 Imperial Valley, California, earthquake. Geophys. Res. Lett. 30 (5) 4 pp.

Lavallée, D., Liu, P., Archuleta, R.J., 2006. Stochastic model of heterogeneity in earthquake slip spatial distributions. Geophys. J. Int. 165 (2), 622–640.

Liu, Y., Lapusta, N., 2008. Transition of Mode II cracks from sub-Rayleigh to intersonic speeds in the presence of favorable heterogeneity. J. Mech. Phys. Solids 56 (1), 25–50.

Liu, P., Archuleta, R.J., Hartzell, S.H., 2006. Prediction of broadband ground-motion time histories: hybrid low/high-frequency method with correlated random source parameters. Bull. Seismol. Soc. Am. 96 (6), 2118–2130.

Liu-Zeng, J., Heaton, T., DiCaprio, C., 2005. The effect of slip variability on earthquake slip-length scaling. Geophys. J. Int. 162 (3), 841–849.

Ma, S., Liu, P., 2006. Modeling of the perfectly matched layer absorbing boundaries and intrinsic attenuation in explicit finite-element methods. Bull. Seismol. Soc. Am. 96 (5), 1779–1794.

Madariaga, R., Olsen, K., 2000. Criticality of rupture dynamics in 3-D. Pure Appl. Geophys. 157 (11), 1981–2001.

Mai, P.M., Beroza, G.C., 2002. A spatial random field model to characterize complexity in earthquake slip. J. Geophys. Res. 107 (B11).

Oglesby, D.D., Day, S.M., 2002. Stochastic fault stress: implications for fault dynamics and ground motion. Bull. Seismol. Soc. Am. 92 (8), 3006–3021.

Olsen, K.B., et al., 2009. Shakeout-D: ground motion estimates using an ensemble of large earthquakes on the southern San Andreas Fault with spontaneous rupture propagation. Geophys. Res. Lett. 36.

Robinson, D.P., Brough, C., Das, S., 2006. The Mw 7.8, 2001 Kunlunshan earthquake: extreme rupture speed variability and effect of fault geometry. J. Geophys. Res. 111 (B08303).

Rosakis, A.J., Samudrala, O., Coker, D., 1999. Cracks faster than the shear wave speed. Science 284 (5418), 1337–1340.

Schmedes, J., Archuleta, R.J., 2008. Near-source ground motion along strike–slip faults: insights into magnitude saturation of PGV and PGA. Bull. Seismol. Soc. Am. 98 (5), 2278–2290.

Schmedes, J., Archuleta, R.J., Lavallee, D., 2010. Correlation of earthquake source parameters inferred from dynamic rupture simulations. J. Geophys. Res. 115, B03304. doi:10.1029/2009JB006689.

Shin, T.C., Kuo, K.W., Lee, W.H.K., Teng, T.L., Tsai, Y.B., 2000. A preliminary report on the 1999 Chi-Chi (Taiwan) earthquake. Seismol. Res. Lett. 71 (1), 24–31.

Sommerville, P., et al., 1999. Characterizing crustal earthquake slip models for the prediction of strong ground motion. Seismol. Res. Lett. 70, 59–80.

Spudich, P., Cranswick, E., 1984. Direct observation of rupture propagation during the 1979 Imperial Valley earthquake using a short baseline accelerometer array. Bull. Seismol. Soc. Am. 74 (6), 2083–2114.

Spudich, P., Frazer, L.N., 1984. Use of ray theory to calculate high-frequency radiation from earthquake sources having spatially variable rupture velocity and stress drop. Bull. Seismol. Soc. Am. 74 (6), 2061–2082.

Wu, F., Thomson, K.C., Kuenzler, H., 1972. Stick-slip propagation velocity and seismic source mechanism. Bull. Seismol. Soc. Am. 62 (6), 1621–12658.